Consensus-Based Image Segmentation via Topological Persistence

Qian Ge* and Edgar Lobaton*
Department of Electrical and Computer Engineering
North Carolina State University, Raleigh, North Carolina 27695-7911
{qge2, edgar.lobaton}@ncsu.edu

Abstract

Image segmentation is one of the most important low-level operation in image processing and computer vision. It is unlikely for a single algorithm with a fixed set of parameters to segment various images successfully due to variations between images. However, it can be observed that the desired segmentation boundaries are often detected more consistently than other boundaries in the output of state-of-the-art segmentation results. In this paper, we propose a new approach to capture the consensus of information from a set of segmentations generated by varying parameters of different algorithms. The probability of a segmentation curve being present is estimated based on our probabilistic image segmentation model. A connectivity probability map is constructed and persistent segments are extracted by applying topological persistence to the probability map. Finally, a robust segmentation is obtained with the detection of certain segmentation curves guaranteed. The experiments demonstrate our algorithm is able to consistently capture the curves present within the segmentation set.

1. Introduction

Image segmentation is one of the most important low-level operation in image processing and computer vision. The existing techniques cluster the image pixels into a set of groups visually distinct and uniform with respect to some properties, such as gray level, texture or color [11]. There are a variety of algorithms that have been proposed for image segmentation. Grouped by their methodology, segmentation algorithms can be mainly divided into these classes: edge-based segmentations [2, 13] make use of edge information to segment regions in an image; superpixel-based segmentations [20, 17, 23] use superpixels as initialization of segmentation to make use of superpixel cues and reduce computational complexity; and graph-based segmentations [25, 21, 9] represent the image as a weighted undirected graph for which the segmentation problem is treated as a graph partitioning problem.

State-of-the-art segmentation algorithms are able to successfully capture different features from images. However, it is difficult for a single algorithm with the same parameters to segment all the images successfully due to variations between images. One feature that may be observed is that when comparing the segmentation results from different algorithms with different parameters, the desired boundaries are detected more consistently than other boundaries. One example is shown in Fig. 1 (b). The four segmentations are generated by four different algorithms. The boundary of the swan is detected in all the results with a small perturbation from each other. Thus, extracting consistent detections of a set of segmentations can give a better estimation of correct segmentation.

In this paper, we propose a new approach to capture the consensus segmentation information from a set of segmentations generated by varying parameters of different segmentation algorithms. First, the probability of a segmentation curve present around a location x is estimated based on our image segmentation model and a connectivity probability map is constructed. Then, persistent segments are extracted by applying topological persistence to the probability map. Finally, a robust segmentation is obtained with the guarantee of detection of certain segmentation curves. Our approach is illustrated in Fig. 1.

The rest of the paper is organized as follows: Section 2 gives an overview of the related work; Section 3 introduces our image segmentation model; A detailed description of the proposed segmentation approach is introduced in Section 4; Section 5 discusses the choice of thresholds; Experiments of our method are discussed in Section 6; Finally, section 7 summarizes the paper and discusses future scope.

2. Related Work

In this section we briefly overview the image segmentation approaches based on consensus algorithms.

In [18], the segmentation set is generated by many runs

*This work was partially supported by the National Science Foundation under award CNS-1239323.

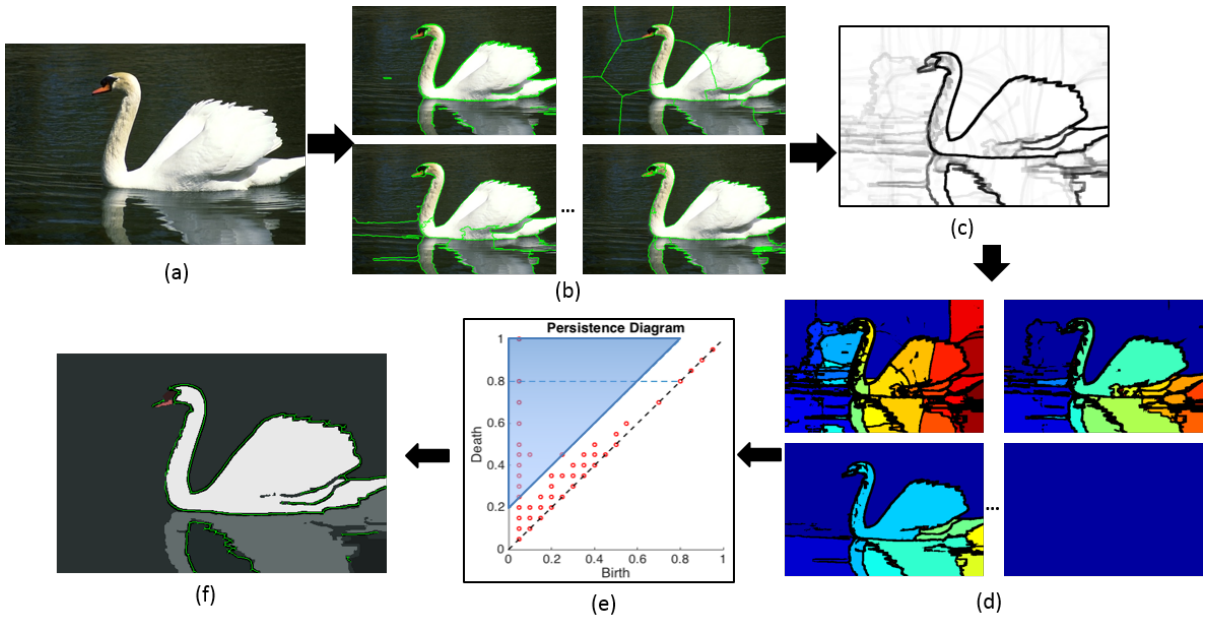

Figure 1. Pipeline of the proposed approach. (a) Original image. (b) Four samples from the segmentation set. The segmentation set generated by varying parameters of four algorithms are used as an input set. (c) A connectivity probability map is constructed. (d) A set of labeled images, which corresponds to the filtration set for the topological persistence analysis, is generated by thresholding the connectivity probability map. (e) Persistence diagram of the filtration shown in (d) where each point in the diagram corresponds to a connected component in the filtration. (f) Segmentation result obtained by applying two thresholds in the persistence diagram.

of a randomized segmentation algorithm. The closed contours are then obtained by combining those segmentation through consensus region merging. In [19], a consensus segmentation algorithm applied on remotely sensed images is introduced, using a stochastic optimization algorithm based on the Filtered Stochastic BOEM (Best One Element Move) method. Also, it gives a way to estimate the optimum number of the clusters in segmentation. An unsupervised approach of consensus segmentation based on the graph cuts using the consensus inferred from hierarchical segmentation ensembles for partitioning images into foreground and background regions is presented in [12] . In [10], the segmentation set is used for computing a superpixel image, which is used to generate consensus clustering. In [22], the authors propose a bi-clustering framework and perspective for reaching consensus in grouping problems, which can be used in consensus image segmentation. In [16], a cluster ensemble is used to determine the number of clusters in a group of data, which can be used to estimate the number of regions in the segmentation.

3. Image Segmentation Model

Let $\Omega \subset \mathbb{R}^2$ be the image domain. We represent a segmentation $\mathcal{S}$ of an image as a set X of nodes $x_i \in \Omega$, and a set Γ of continuous curves $\gamma_{ij} : [0,1] \to \Omega$ for which $\gamma_{ij}(0) = x_i$ and $\gamma_{ij}(1) = x_j$. Each curve is non-intersecting with any curve in the set and the number of curves incident with any point is greater than one, making this a valid segmentation. The segmentation $\mathcal{S}$ has a graphical structure corresponding to a planar graph $\mathcal{G} = (V, E)$ where $V = \{1, \cdots, N_X\}$, N_X is the number of nodes in X, and $E = \{(i,j) \,|\, \gamma_{ij} \in \Gamma\}$. We define a segmentation $\mathcal{S}$ by the pair $(\mathcal{G}, \Gamma)$.

In order to define a probabilistic model for segmentations, the unknown generative model is represented as:

$$P[\mathcal{S} = (\mathcal{G}, \Gamma)] = P[\Gamma \,|\, \mathcal{G}] \cdot P[\mathcal{G}]. \tag{1}$$

It is assumed that the graphical structure $\mathcal{G}$ is obtained from an over-segmentation of the image with corresponding set of vertices V_o and edges E_o. First, a subset of edges $E \subset$

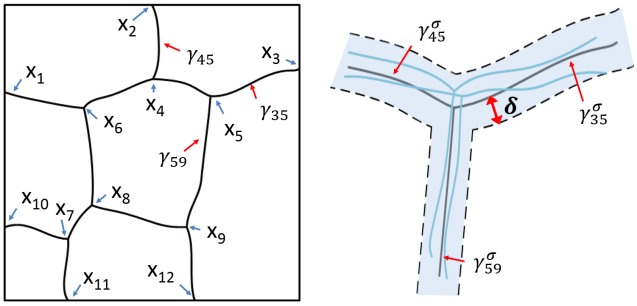

Figure 2. Illustration of the model used for segmentations: The representation model for a segmentation $\mathcal{S}$ (left) and the bounded perturbation model around $\mathcal{S}_\sigma$.

E_o is selected and the vertices $V \subset V_o$ corresponding to the subgraph induced by E are chosen. We let

$$p_{ij} := P\left[(i,j) \in E\right], \tag{2}$$

which is a piece of information from this unknown distribution of graphical models that will be used in our study. The probabilities p_{ij} specify the probability of a curve segment to be present. We further assume that given a graphical structure, the set of curves Γ is generated using some process that does not violate the graphical structure (i.e., it does not introduce intercepts between the curves).

Let us define $\mathcal{G}_\sigma$ as the graph obtained by selecting the set of edges $E_\sigma = \{(i,j) \in E_o \,|\, p_{ij} > \sigma\}$ and corresponding nodes V_σ. We assume that there exist constants δ and an associated set Γ_σ of curves γ_{ij}^σ that satisfy

$$|\gamma_{ij} - \gamma_{ij}^\sigma|_\infty \leq \delta \quad \text{for all} \quad (i,j) \in E_\sigma \cap E \tag{3}$$

for any segmentation with graphical structure $\mathcal{G} = (V, E)$, where $|f_1 - f_2|_\infty = \sup_{s\in[0,1]} ||f_1(s) - f_2(s)||_2$. This assumption requires the set of realizations of a given curve γ_{ij} to be concentrated within a band of radius δ around the curve $\gamma_{ij}^{\sigma,\delta}$. We define $\mathcal{S}_\sigma = (\mathcal{G}_\sigma, \Gamma_\sigma)$.

Our objective is to come up with a procedure and a set of conditions under which the segmentation $\mathcal{S}_\sigma$ can be estimated. In particular, we introduce a procedure under which we can construct a subset $\mathcal{C} \subset \Omega$ such that $im(\mathcal{S}_\sigma) \subset \mathcal{C}$, where $im(\mathcal{S}_\sigma) = \bigcup_{(i,j)\in E_\sigma} im(\gamma_{ij}^\sigma)$ and $im(\gamma_{ij}^\sigma) = \left\{x = \gamma_{ij}^\sigma(s) \in \Omega \,|\, s \in [0,1]\right\}$.

Let $D_\delta : \Omega \to [0,1]$ be the function that measures the probability of having a segmentation overlapping with a ball $B_\delta(x)$ of radius δ centered at a point x. That is,

$$D_\delta(x) := P\left[im(S) \cap B_\delta(x) \neq \emptyset\right]. \tag{4}$$

Theorem 1. *The set $\mathcal{C} = \{x \,|\, D_\delta(x) \geq \sigma\}$ satisfies:*

$$im(\mathcal{S}_\sigma) \subset \mathcal{C} \tag{5}$$

and

$$im(\mathcal{S}_\sigma)^c \ominus B_{2\delta} \subset \mathcal{C}^c, \tag{6}$$

where $\mathcal{C}^c$ is the complement of set $\mathcal{C}$ in Ω, $B_{2\delta}$ is the ball of radius 2δ and $\ominus$ operator is the morphological erosion operator.

Proof. For the first inequality it is sufficient to show that every point in $\mathcal{S}_\sigma$ has $D_\delta(x) \geq \sigma$. Let $x \in im(\mathcal{S}_\sigma)$. Then, we have that given $(i,j) \in E$ then $B_\delta(x)$ will intersect with $im(\gamma_{ij})$ due to Eqn 3. Noting that $(i,j) \in E$ with probability greater that σ (by definition of S_σ) then $D_\delta(x) \geq \sigma$.

For the second inequality, we note that any point x that is more than 2δ from $im(\mathcal{S}_\sigma)$ has $D_\delta(x) = 0$ since no curves will intersect with the ball $B_\delta(x)$. □

4. Approach

In this section, we describe our approach in detail. We use the connectivity of an $n \times n$ patch to construct a disconnection probability map $D_n^*(x)$. Then we discuss how the size n of the patch affects the quality of the model approximation. The size of the patch is a parameter associated with the perturbation bound δ in our model.

4.1. Boundary characterization

Given a set of segmentations $\{\mathcal{S}_k, k = 1, \ldots, K\}$ generated by different segmentation algorithms with different parameters, we assume that the segment curves appearing in the set satisfy the probabilistic model we define in Section 3. That is, each segment curve in the segmentation results corresponds to an edge $(i,j) \in E_o$ of the over-segmentation.

In a segmentation $\mathcal{S}_k$, an $n \times n$ patch $N(x)$ centered at x is called connected if all the pixels in the patch have the same label. Then the number of times it is disconnected over the set $\{\mathcal{S}_k\}$, C_n^{dis}, counts how many times one or more segment curves appear within that patch. As shown in Fig. 3, a large patch may capture more than one edge in E_o, while too small of a patch may miss some parts of the segment curves in E_o. Based on our model, we have $D_n^*(x) = C_n^{dis}/K$ as an estimate for $D_\delta(x)$. We assume that segment curves of the desired segmentation boundary are more consistent than undesired ones in set $\{S_k\}$ with a small perturbation around the correct boundary. Therefore, high values of $D_\delta(x)$ indicate the high confidence of a segment curve corresponding to $(i,j) \in E_o$ along the patch in the groundtruth.

When applying a threshold σ, then a labeled image $L(n,\sigma)$ is obtained by computing the connected components of the set $\mathcal{L}_\sigma^n = \{x \,|\, D_n^*(x) \leq \sigma\}$. Changing σ from $\sigma_{min} = 0$ to $\sigma_{max} \leq 1$ produces a set of labeled image $\{L(n,\sigma)\}_{\sigma\in[0,\sigma_{max}]}$. The connected components appearing at high σ values indicate high probability of segment curves between them. One example of the labeled image set is shown in Fig. 6 (i)-(l).

4.2. Choice of Parameter n

As mentioned in Section 4.1, the quality of approximation of the segmentation model depends on the parameter n. As shown in Fig. 6 (i)-(l), the connected components get larger and merged as σ increases. Two connected components will merge under a certain σ if there is a path of overlapped patches connecting them. If γ_{ij} for $(i,j) \in E_o$ is present between the two connected components with probability p_{ij}, then p_{ij} can be approximated by the minimum valued of σ that merges the two connected components.

In order to analyze the effect on the choice of the parameter n, consider an image with two segments separated by a soft vertical edge. Assume γ_{ij} for $(i,j) \in E_o$ is present

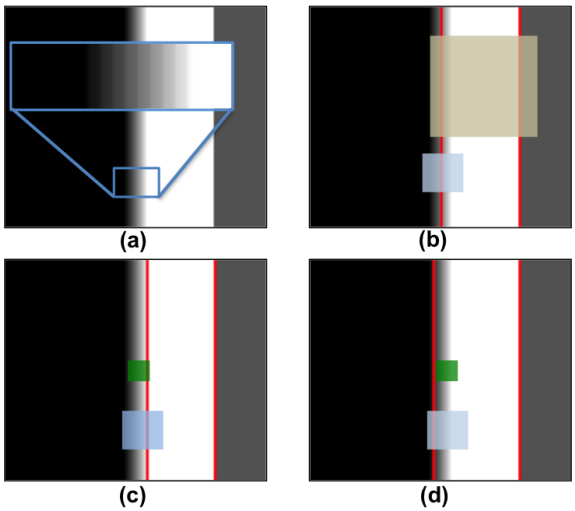

Figure 3. Example of segment curves captured by patches. (a) An image with a soft edge and a sharp edge. (b)-(d) show three possible segmentation results. Red lines are the detected segment curves. (b) The large brown patch covers two segment curves. The present probability of neither edge can be measured correctly by the patch of that size. The smaller blue patch is a suitable choice. (c)-(d) The small green patch cannot cover all the segment curves of the soft edge, which makes it have lower disconnection probability than the actual value, whereas the blue patch is a suitable choice since it covers all the possible positions of the curves.

within a range of 2δ pixels with probability p_{ij} (i.e., a distance of δ from its centerline). Finding the minimum value of σ that captures the separation between opposite sides of the regions separated by γ_{ij} requires a value of n that is big enough for this purpose. For the case $n-2 \geq 2\delta$, the range of variations of the segments can be covered by a single $n \times n$ patch as shown in Fig. 4 (a). The pixel x in the middle of the range has the disconnection probability $D_n^*(x) = p_{ij}$. The minimum probability threshold that makes the two segments connected is $\sigma = p_{ij}$. For the case $n-2 < 2\delta$, a single $n \times n$ patch cannot cover the entire range, which makes the disconnection probability $D_n^*(x) < p_{ij}$. Note that the cross-sectional range can be covered by $m = [\frac{2\delta+1}{n-1}]$ patches overlapping with one pixel, where $[a]$ is the minimum integer greater or equal to a. Fig. 4 (b) shows one example of this case. Let p_d^k be the disconnected probability of k-th patch. The disconnection probabilities satisfy $\sum_{k=1}^{m} p_d^k = p_{ij}$, where the sum is over the patches. There exists at least one pixel x along the cross-sectional line for the range of variation of γ_{ij} with $D_n^*(x) \geq p_{ij}/m$. The probability threshold that ensures that the two segments are disconnected is $\sigma < p_{ij}/m$. Thus, if n is chosen large enough, say $n-2 \geq 2\delta$, then $(i,j) \in E_o$ with γ_{ij} appearing within range 2δ in the set $\{\mathcal{S}_k\}$ with probability p_{ij} will be represented in all the labeled images with $\sigma < p_{ij}$. For $(i,j) \in E_o$ with range $2\delta > n-2$, they will be represented in the label image with $\sigma < \sigma'$, where $p_{ij}/m \leq \sigma' < p_{ij}$ and $m = [\frac{2\delta+1}{n-1}]$.

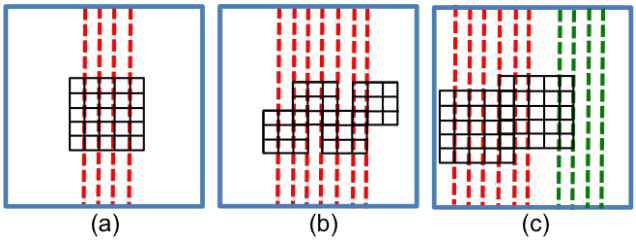

Figure 4. Illustration of the effect of the choice of n. Vertical dash lines with the same color indicate the variation regions of one segment curve γ. (a) The case of $n-2 \geq 2\delta$. The variation region can be covered by one patch. (b) The case of $n-2 < 2\delta$. The variation region can be covered by four patches in this example. (c) The case of closed segment curves influence the approximation.

Let us consider another case corresponding to two segment curves γ_{ij} and $\gamma_{i'j'}$ where (i,j) and $(i',j') \in E_o$ are close to each other. An example is shown in Fig. 4 (c). The red dash lines represent the range for γ_{ij} and the green is for $\gamma_{i'j'}$. Assume that, when $\gamma_{i'j'}$ is not present, $D_n^*(x) = \sigma_0$ where x is the center of right patch in the figure and σ_0 is the minimum σ making the two segments separated by red curve merge. After adding $\gamma_{i'j'}$, the probability of having a disconnected set increases, since $\gamma_{i'j'}$ is present in the area covered by the right patch. That is, $D_n^*(x) > \sigma_0$. Therefore, $\gamma_{i'j'}$ near γ_{ij} may make the minimum connection threshold for γ_{ij} greater than its actual value. For an $n \times n$ patch, segment curves which have perturbation regions with ranges that are at least $n-1$ pixels away from each other can be identified without the influence of other segment curves.

5. Thresholding

In the set of labeled images $\{L(n,\sigma)\}_{\sigma \in [0,\sigma_{max}]}$, the connected components get larger and merged with other connected components as σ increases. To estimate the segmentation $\mathcal{S}_\sigma$, we extract the connected components by applying a threshold σ on $D_n^*(x)$ as well as selecting only those regions that have a topological persistence greater than τ. This last step ensures that regions that are possibly generated by errors in the estimation of $D_\delta(x)$ are not considered.

5.1. Disconnection Threshold σ

The threshold σ is used to get the segment curve γ_{ij} with probability $p_{ij} \geq \sigma$. As discussed in Section 4.2, the quality of the approximation of the segmentation model is based on the size n of patch. In order to capture all the segment curves that are present with probability greater than p_{ij}, given that we only care about the curves appearing within a range $2\delta \leq n-2$, we can set the threshold $\sigma = p_{ij}$. If we consider the curves that appear within a larger range

$2\delta > n-2$, the threshold should be $\sigma = p_{ij}/m$, where $m = [\frac{2\delta+1}{n-1}]$.

5.2. Persistence Threshold τ

If a single value of σ is used for thresholding, the segment curves are estimated by only one labeled image $L(n,\sigma)$ and we throw out the information of other labeled images in the set. Also, the ideal value of p_{ij} and δ to get a reasonable segmentation may be different due to the variations of the image quality over the dataset. Images with blurred edges require large δ and low p_{ij} while images with sharp edges require small δ and have high p_{ij}. Furthermore, the connected components we want to extract correspond to the peaks of the connectivity probability map $1 - D_n^*$, simply thresholding D_n^* may not capture all the desired regions. To address this, we apply topological persistence to generate more robust segmentation estimation. This technique has been used in some previous works [24, 3] to get the robust obstacle segmentation from stereo pairs. In this section, we briefly introduce the concept of topological persistence and discuss how it applies to our image segmentation process. A comprehensive review of topological persistence can be found in [7].

5.2.1 Background

Consider a function $f : \mathbb{R}^2 \to [0,1]$ defined over a 2D domain. Given a threshold value $\sigma \in [0,1]$, the upper level set of f is defined as $\mathcal{E}_\sigma = f^{-1}[1-\sigma, 1]$. The set $\mathcal{E}_\sigma = f^{-1}[1-\sigma, 1]$ is a filtration and satisfies:

$$\mathcal{E}_{\sigma_1} \subseteq \mathcal{E}_{\sigma_2} \qquad \text{whenever} \qquad \sigma_1 \leq \sigma_2. \tag{7}$$

Persistent homology [6] focuses on connected components during the filtration of upper level sets of f.

The topological features for our application are the connected components in set $\mathcal{E}_\sigma$, and each is summarized by the appearance and disappearance (i.e. merging with other connected components) of a connected component during a filtration; this is referred to as the birth (b_k) and death (d_k) times of the k-th feature, respectively. Each feature can be encoded by a point (b_k, d_k) and the diagram with all features represented as a set of point is called persistence diagram. The persistence interval of k-th feature is measured by $d_k - b_k$.

Fig. 5 shows an example of such function f. At $\sigma = 0.15$, there exists two connected components. A small connected component is born at $\sigma = 0.25$. When $\sigma = 0.35$, the one born at $\sigma = 0.25$ dies because it merges with another connected component which has an earlier birth time, leading to a persistence interval of length 0.1. At $\sigma = 0.6$, all connected components merge to the biggest one. All the connected components die at this time except the one having the earliest birth time. A persistence diagram which

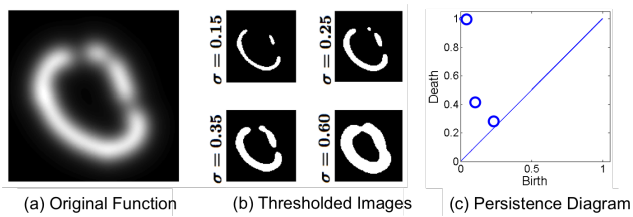

(a) Original Function (b) Thresholded Images (c) Persistence Diagram

Figure 5. Persistence analysis. (a) Original image. (b) Image after thresholding. (c) Persistence Diagram.

encodes the birth and death time of each region can be used to select the persistent region. The diagram corresponding to this example is shown in Fig. 5 (c). The further away a feature is from the diagonal the higher is its persistence and robustness to perturbations.

5.2.2 Extract Persistence Connected Components

In order to extract the persistent connected components for our segmentation process, we first define a connection probability map $f(x) = 1 - D_n^*(x)$. Then, the labeled image set $\{L(n,\sigma)\}_{\sigma\in[0,\sigma_{max}]}$ form a filtration of the upper level set of f. Fig. 6 (g) shows the persistence diagram extracted from the filtration shown in Fig. 6 (i)-(l). Only the regions with persistence intervals greater than τ are kept to avoid the connected components generated by noise in the segmentation set $\{S_k\}$. This threshold is illustrated by a blue dash line parallel to the diagonal in Fig. 6 (g). The size of each region above the persistence threshold can vary, since it exists over a range of τ. To get the largest size of the persistence region, the largest set of points which is associated with its death time is selected as the segmentation result [24].

One advantage of the persistence diagram is its stability property [4]. Small changes in the function f lead to small changes in the persistence diagram. This translates into the following for our scenario: we can obtain segmentation result that is robust to parameter value changes and small variations in the segmentation set $\{S_k\}$.

To make sure the segment curves γ_{ij} present with probability greater than p_{ij} within a range $2\delta \leq n-2$ can be captured, we can set $\sigma_{max} = p_{ij}$. This ensures that regions with death after p_{ij} will never merge with other regions in filtration $\{L(n,\sigma)\}_{\sigma\in[0,p_{ij}]}$. This threshold is shown as the horizontal blue dash line in Fig. 6 (g). This is equivalent to removing the labeled images with $\sigma > p_{ij}$ from the filtration. For this new diagram, the connected components separated by those segment curves will never get merged in the filtration and will be present in the final segmentation result. Note that this is not the same as simply thresholding $f(x) = 1 - D_n^*(x)$ by $\sigma = p_{ij}$, which will remove the regions with death before σ as well as those that are born after σ.

6. Experiment

The proposed approach is implemented in MATLAB. We use images from the Berkeley Segmentation Database [15, 1] to test our algorithm. There are five groundtruth segmentations per image labeled by different human subjects.

We adapt the segmentation coverage score defined in [1] to evaluate the segmentation result. The overlap score between regions R and R' is defined as

$$O(R, R') = \frac{|R \cap R'|}{|R \cup R'|}, \tag{8}$$

where $|R|$ is the area of R. The covering of a segmentation groundtruth $\mathcal{S}_r$ by a segmentation $\mathcal{S}'$ is defined as:

$$C(\mathcal{S}' \to \mathcal{S}_r) = \frac{1}{N} \sum_{R \in \mathcal{S}_r} |R| \max_{R' \in \mathcal{S}'} O(R, R'), \tag{9}$$

where N is the number of pixels in the image. To combine the information of five groundtruth segmentations, the covering score for segmentation $\mathcal{S}'$ is defined by

$$C(S') = \frac{1}{5} \sum_{k=1}^{5} C(\mathcal{S}' \to \mathcal{S}_r^k) \tag{10}$$

where $\mathcal{S}_r^k$ is the k-th groundtruth segmentation.

6.1. Generation of Segmentation Set

We use segmentation results generated by four algorithms as our input. These four algorithms are SAS [14], Normalized Cuts [21], Graph-based segmentation [8] and Mean Shift [5]. The first two algorithms require the number of regions in the segmentation result as an input parameter. We get 26 segmentations from each of these two algorithms by varying the number of regions from 5 to 30. The Graph-based segmentation uses a Gaussian with standard deviation σ to remove the digitization artifacts and a parameter k to control the scale of observation which affects the size of the segments. We vary σ from 0.4 to 0.8 with step size 0.1 and k from 500 to 5000 with step size 100 to generate 230 segmentations. For Mean Shift, we generate 238 segmentations by changing the spatial search window size and bandwidth of the search window from 2 to 15 with step size 1, and from 7 to 15 with step size 0.5, respectively. These range of parameters were chosen because they generate reasonable but different segmentations for most of the test images.

When computing the disconnection probability map D_n^*, we first compute $D_{n,i}^*$ where $i = 1, 2, 3, 4$ for the i-th algorithm and D_n^* is obtained by taking the average of the $D_{n,i}^*$. This process equally weights the contribution from each algorithm.

6.2. Results

In our experiment, we use $n = 5$ as the patch size. The filtration is generated by varying $\sigma \in [0, \sigma_{max}]$ with step size 0.05. The thresholds we use are $\sigma_{max} = 0.8$ and $\tau = 0.4$. Fig. 6 shows one segmentation result of the proposed approach. Fig. 6 (a)-(d) shows the best segmentation results in the segmentation set of the four algorithms mentioned in Section 6.1 based on the covering score. As we can see, the result of the best score, 0.92, has some small noisy regions and it is not visually better than the result of SAS with score 0.90. This leads us to believe that the covering score may not be the best evaluation metric in this scenario. As a future work, better metrics will need to be identified to better quantify the quality of a segmentation.

Fig. 6 (f) shows the connectivity probability map $1 - D_n^*$. Darker color indicates the lower connection probability of those regions. We note that this map properly captures the contours of the hawk and the branch by assigning them a low connection probability. The locations with high connection probabilities correspond mostly to undesired segmentation curves.

Fig. 6 (i)-(l) shows the labeled images for $\sigma = 0, 0.25, 0.5, 0.8$. For low σ, most of the segment curves appearing in the input segmentation set are captured. However, when σ increases from 0.25 to 0.5, the undesired segmentation curves are removed. For $\sigma_{max} = 0.8$, almost all the remaining segment curves are visually correct.

Fig. 6 (g) shows the persistence diagram of the connected components during filtration. The thresholds are $\sigma_{max} = 0.8$ and $\tau = 0.4$. Connected components corresponding to the points in the blue region are selected as our segmentation result. Since the size of persistent connected components can vary in a range of τ, we select the set of points associated with the death time as the segmentation result. This maximizes the size of the k-th persistent region and captures the curves with probability greater than 0.8.

Fig. 6 (h) shows our segmentation result. Each region is colored by its average value in the region. Since the covering set that we built is not an actual segmentation, we recover a segmentation by extracting the skeleton of the covering set, which is shown in green in the image. It is observed that this approach maintains the segmentation curves that are visually desirable.

Fig. 7 shows more results of our proposed approach, which is able to extract the segment curves that appear with high probability in the input segmentation set. The covering score of the proposed approach is not better than the best score in the segmentation set. One reason for this is that the results have some unlabeled regions. However, the proposed approach tends to segment single object into smaller number of regions which may be divided into more regions by the base approaches. This is because the edges are randomly detected inside an object due to the similarity within

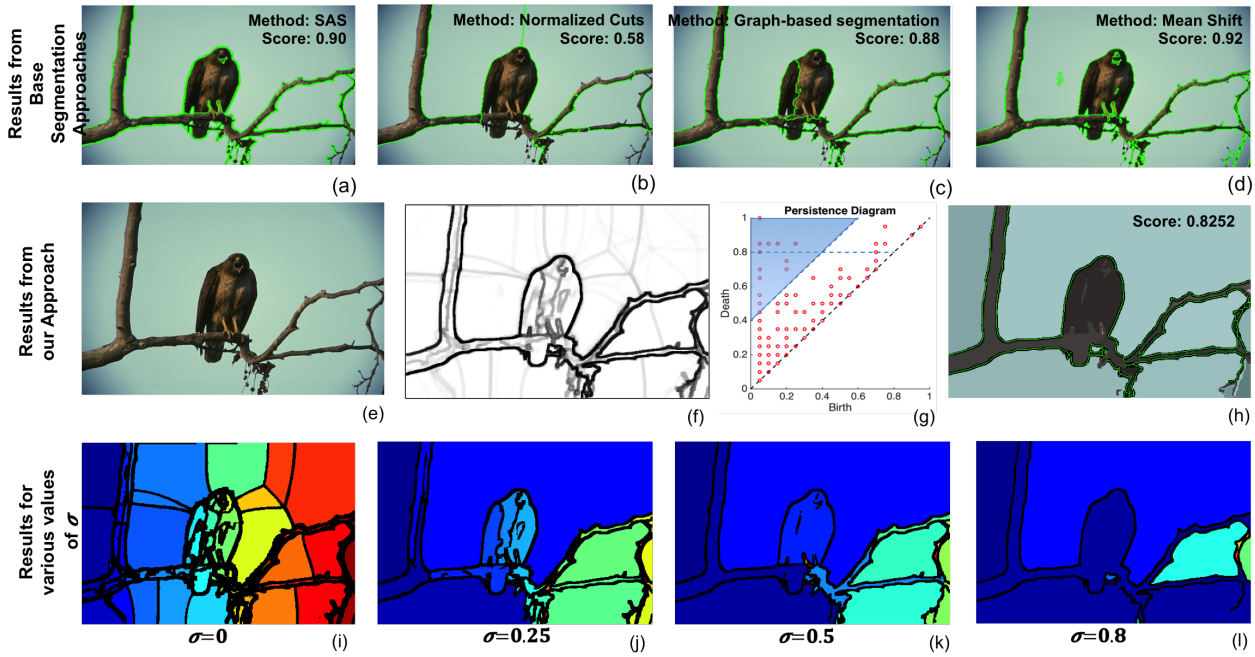

Figure 6. (a)-(d) Results with best covering score for base segmentation approaches in the input segmentation set: SAS [14], Normalized Cuts [21], Graph-based segmentation [8] and Mean Shift [5]. (e) Original image. (f) Connection probability map. (g) Persistence diagram of the connected components during filtration. The thresholds are $\sigma_{max} = 0.8$ and $\tau = 0.4$. (h) Our segmentation result. The green curves are the skeleton of the regions without label. (i)-(l) Filtration with $\sigma = 0, 0.25, 0.5, 0.8$. With σ increasing, the regions separated by segment curves with low probability are merged early.

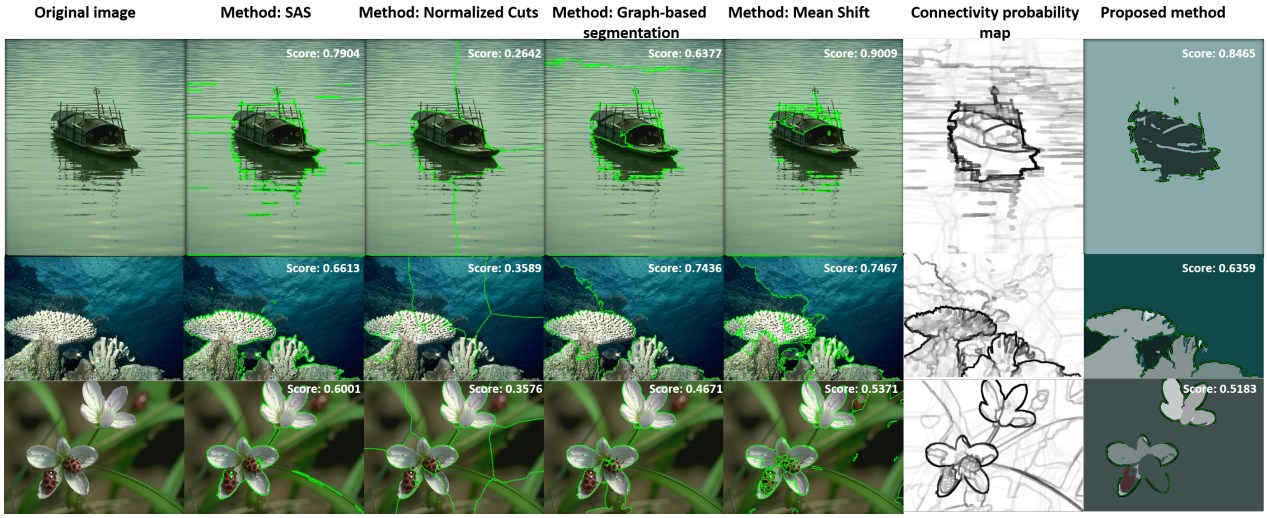

Figure 7. Best segmentation results of the four base-algorithms in the segmentation set and result of proposed algorithm. Left to right: Original image, SAS [14], Normalized Cuts[21], Graph-based segmentation [8], Mean Shift [5], connection probability map, and proposed algorithm.

the region of that object. For the same reason, we can remove the curves generated in the background. However, if an undesired curve is always detected by all the algorithm, our approach will fail since our model assumes that frequently detected curves are valid segmentation curve.

7. Conclusion

In this paper, we propose a new approach to capture the consensus segmentation information from a set of segmentations generated by varying parameters of different algorithms. The probability of a segmentation curve being present is estimated based on our probabilistic image seg-

mentation model. A connection probability map is constructed to characterize the segmentation curves with high probability. Then, persistence segments are extracted by applying topological persistence to the probability map. Finally, a robust segmentation is obtained with the detection of certain segmentation curves guaranteed. The experiments demonstrate our algorithm is able to capture the curves present consistently within the segmentation set.

In the future, we will extend our model and approach by considering multiple neighborhoods of size $n \times n$ (i.e., treating n as another parameter). Also, we hope to improve the segmentation result by identifying ways to select an appropriate range of parameters for the base segmentation algorithms, and a good estimate for the persistence threshold τ via training using user-input.

References

[1] P. Arbelaez, M. Maire, C. Fowlkes, and J. Malik. Contour detection and hierarchical image segmentation. *IEEE Trans. Pattern Anal. Mach. Intell.*, 33(5):898–916, May 2011. 6

[2] J. Canny. A computational approach to edge detection. *Pattern Analysis and Machine Intelligence, IEEE Transactions on*, PAMI-8(6):679–698, Nov 1986. 1

[3] S. Chattopadhyay, Q. Ge, C. Wei, and E. Lobaton. Robust multi-target tracking in outdoor traffic scenarios via persistence topology based robust motion segmentation. In *2015 IEEE Global Conference on Signal and Information Processing (GlobalSIP)*, pages 805–809, Dec 2015. 5

[4] D. Cohen-Steiner, H. Edelsbrunner, and J. Harer. Stability of persistence diagrams. *Discrete Comput. Geom.*, 37(1):103–120, Jan. 2007. 5

[5] D. Comaniciu and P. Meer. Mean shift: a robust approach toward feature space analysis. *IEEE Transactions on Pattern Analysis and Machine Intelligence*, 24(5):603–619, May 2002. 6, 7

[6] H. Edelsbrunner and J. Harer. Persistent homology-a survey. *Contemporary mathematics*, 453:257–282, 2008. 5

[7] H. Edelsbrunner and J. Harer. *Computational Topology - an Introduction*. American Mathematical Society, 2010. 5

[8] P. F. Felzenszwalb and D. P. Huttenlocher. Efficient graph-based image segmentation. *International Journal of Computer Vision*, 59(2):167–181. 6, 7

[9] G. Floros and B. Leibe. Joint 2d-3d temporally consistent semantic segmentation of street scenes. In *Computer Vision and Pattern Recognition (CVPR), 2012 IEEE Conference on*, pages 2823–2830, June 2012. 1

[10] L. Franek, D. D. Abdala, S. Vega-Pons, and X. Jiang. *Computer Vision – ACCV 2010: 10th Asian Conference on Computer Vision, Queenstown, New Zealand, November 8-12, 2010, Revised Selected Papers, Part IV*, chapter Image Segmentation Fusion Using General Ensemble Clustering Methods, pages 373–384. Springer Berlin Heidelberg, Berlin, Heidelberg, 2011. 2

[11] J. Freixenet, X. Muoz, D. Raba, J. Mart, and X. Cuf. Yet another survey on image segmentation: Region and boundary information integration. In A. Heyden, G. Sparr, M. Nielsen, and P. Johansen, editors, *Computer Vision ECCV 2002*, volume 2352 of *Lecture Notes in Computer Science*, pages 408–422. Springer Berlin Heidelberg, 2002. 1

[12] H. Kim, J. J. Thiagarajan, and P. T. Bremer. Image segmentation using consensus from hierarchical segmentation ensembles. In *Image Processing (ICIP), 2014 IEEE International Conference on*, pages 3272–3276, Oct 2014. 2

[13] S. Konishi, A. Yuille, J. Coughlan, and S.-C. Zhu. Statistical edge detection: learning and evaluating edge cues. *Pattern Analysis and Machine Intelligence, IEEE Transactions on*, 25(1):57–74, 2003. 1

[14] Z. Li, X.-M. Wu, and S.-F. Chang. Segmentation using superpixels: A bipartite graph partitioning approach. In *IEEE International Conference on Computer Vision and Pattern Recognition (CVPR)*, 2012. 6, 7

[15] D. Martin, C. Fowlkes, D. Tal, and J. Malik. A database of human segmented natural images and its application to evaluating segmentation algorithms and measuring ecological statistics. In *Proc. 8th Int'l Conf. Computer Vision*, volume 2, pages 416–423, July 2001. 6

[16] C. D. Meyer, S. Race, and K. Valakuzhy. Determining the number of clusters via iterative consensus clustering. In *SDM*, pages 94–102. SIAM, 2013. 2

[17] A. Moore, S. Prince, J. Warrell, U. Mohammed, and G. Jones. Superpixel lattices. In *Computer Vision and Pattern Recognition, 2008. CVPR 2008. IEEE Conference on*, pages 1–8, June 2008. 1

[18] F. Nielsen and R. Nock. Consensus region merging for image segmentation. In *Pattern Recognition (ACPR), 2013 2nd IAPR Asian Conference on*, pages 325–329, Nov 2013. 2

[19] M. Ozay, F. T. Yarman-Vural, S. R. Kulkarni, and H. V. Poor. Fusion of image segmentation algorithms using consensus clustering. *CoRR*, abs/1502.05435, 2015. 2

[20] X. Ren and J. Malik. Learning a classification model for segmentation. In *Computer Vision, 2003. Proceedings. Ninth IEEE International Conference on*, pages 10–17 vol.1, Oct 2003. 1

[21] J. Shi and J. Malik. Normalized cuts and image segmentation. *IEEE Trans. Pattern Anal. Mach. Intell.*, 22(8):888–905, Aug. 2000. 1, 6, 7

[22] M. Tepper and G. Sapiro. A bi-clustering framework for consensus problems. *CoRR*, abs/1405.6159, 2014. 2

[23] O. Veksler, Y. Boykov, and P. Mehrani. Superpixels and supervoxels in an energy optimization framework. In K. Daniilidis, P. Maragos, and N. Paragios, editors, *Computer Vision ECCV 2010*, volume 6315 of *Lecture Notes in Computer Science*, pages 211–224. Springer Berlin Heidelberg, 2010. 1

[24] C. Wei, Q. Ge, S. Chattopadhyay, and E. Lobaton. Robust obstacle segmentation based on topological persistence in outdoor traffic scenes. In *Computational Intelligence in Vehicles and Transportation Systems (CIVTS), 2014 IEEE Symposium on*, pages 92–99, Dec 2014. 5

[25] Z. Wu and R. Leahy. An optimal graph theoretic approach to data clustering: theory and its application to image segmentation. *Pattern Analysis and Machine Intelligence, IEEE Transactions on*, 15(11):1101–1113, Nov 1993. 1